Polymer-Layered Silicate Nanocomposite Membranes for Fuel Cell Application

22

Ananta Kumar Mishra, Tapas Kuila, Nam Hoon Kim, and Joong Hee Lee

Contents

1 Introduction 482
2 Development of Polymer Membranes for Fuel Cell Applications 484
3 Proton Conduction Mechanism in Membrane 486
4 Surface Modifications of Nanoclays 487
5 Fabrication of Polymer-Clay Nanocomposite Membranes for Fuel Cell Applications 488
6 Effects of Modifications on the Physical Properties of the Hybrid Membranes 489
6.1 Permeability 489
6.2 Mechanical Properties 492
6.3 Thermal Stability 493
6.4 Water Uptake 495
6.5 Proton Conductivity 496
6.6 Cell Performance 499
7 Summary and Future Direction 505
References 506

A.K. Mishra
BIN Fusion Team, Department of Polymer and Nano Science and Technology, Chonbuk National University, Jeonju, Jeonbuk, Republic of Korea

T. Kuila
Department of BIN Fusion Technology, Chonbuk National University, Jeonju, Jeonbuk, Republic of Korea

N.H. Kim
Department of Hydrogen and Fuel Cell Engineering, Chonbuk National University, Jeonju, Jeonbuk, Republic of Korea

J.H. Lee (✉)
Advanced Wind Power Research Center, Department of Polymer and Nano Science and Technology, Chonbuk National University, Jeonju, Jeonbuk, Republic of Korea

Department of BIN Fusion Technology, Chonbuk National University, Jeonju, Jeonbuk, Republic of Korea
e-mail: jhl@jbnu.ac.kr

J.K. Pandey et al. (eds.), *Handbook of Polymernanocomposites. Processing, Performance and Application – Volume A: Layered Silicates*, DOI 10.1007/978-3-642-38649-7_13,

Abstract

Fuel cells have gained increasing interest in this realm due to their promising emission-free energy generation capability. Proton exchange membrane fuel cells (PEMFCs) and direct methanol fuel cells (DMFCs) are the most suitable candidates for this purpose due to their wide range of energy generation capability. The polymer membranes used in PEMFCs and DMFCs play vital role in transporting the protons from anode to cathode. Nafion is the most widely used and commercialized membrane for this application at low-temperature and highly humidified conditions. The drawbacks associated with low-temperature PEMFCs (heat and water management, CO catalyst poisoning, and fuel crossover) can be avoided by increasing the operating temperature of the fuel cells. However, the drastic decrease in the conductivity of Nafion above 80 °C and low humidity has paved the path towards the development of new membranes and technologies. Additions of layered silicates to the polymer membranes have been observed to be beneficial in this regard owing to their high hydrophilicity, low cost, easy availability, and barrier property towards fuel crossover. The resulting composite membranes also infer improved mechanical and thermal properties, along with water uptake of the membranes escorting towards superior performance of the nanocomposite membranes at high temperature compared to the virgin membrane.

Keywords

Cell Performance • Fuel Cell • Membrane • Nanocomposite • Proton Conductivity

1 Introduction

Energy is highly essential for the growth of the modern society due to its requirements by most of the modern technologies. The main source of power in the present circumstances is the nonrenewable fossil fuels. The limited resource and emission of toxic gases from fossil fuels have prompted to the invention of new techniques of power generation. The green techniques adopted for the energy generation are insufficient for this purpose. Fuel cells have emerged as a new emission-free technology to fulfill the power requirements. It involves the direct conversion of chemical energy into electrical energy by avoiding the intermediate steps required by diesel power generators (Fig. 22.1). Hence, fuel cells can minimize the power losses associated with other power generators [1].

Sir William Robert Grove has invented the first fuel cell in 1839 [1]. It was based on the electrochemical conversions of hydrogen and oxygen into electricity and water [2–4]. This has directed towards the development of several fuel cells, namely, proton exchange membrane fuel cell (PEMFC), direct methanol fuel cell (DMFC), solid oxide fuel cell, alkaline fuel cell, molten carbonate fuel cell, etc. [5–14]. Among these fuel cells, PEMFC possesses wide range of energy generation capability, whereas DMFC possesses the merit of longer operational lifetime and the ability to refuel.

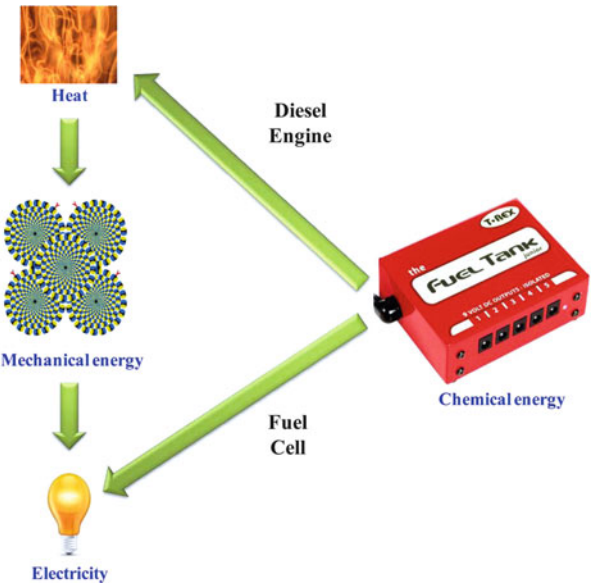

Fig. 22.1 Electricity generation in a diesel engine and fuel cell (see Ref. [1])

In both PEMFC and DMFC, the catalytically oxidized proton at the anode is dragged towards the cathode through a polymer membrane, and simultaneously, the electron generated at the anode moves towards the cathode through an external electrical circuit. The combination of the transmitted protons, electrons, and the reduced oxygen at the cathode surface generate water. However, the electron transmitted through the external electrical circuit is responsible for the generation of electricity [1, 7, 8]. The schematic depiction of PEMFC and DMFC is shown in Figs. 22.2 and 22.3, respectively. The sources of proton in the case of PEMFC and DMFC are hydrogen (H_2) gas and dilute methanol, respectively. The mechanism of proton generation in PEMFCs and DMFCs is shown in Eqs. 22.1 and 22.2, respectively.

$$H_2 \rightarrow H^+ + e^- \tag{22.1}$$

$$2CH_3OH + H_2O \rightarrow 6H^+ + 6e^- + CO_2 \tag{22.2}$$

The role of the membrane in both PEMFC and DMFC is to provide a path for proton conduction from anode to cathode. Hence, limited numbers of membranes are suitable for these applications due to the insulating nature of polymers towards protons. The main requirements of polymer membranes suitable for fuel cell applications include high proton conductivity, good electrical insulation, high thermomechanical and chemical (oxidative and hydrolytic) stability, cost-effectiveness, good barrier property, low swelling stresses, and capability for membrane electrode assembly (MEA) fabrication.

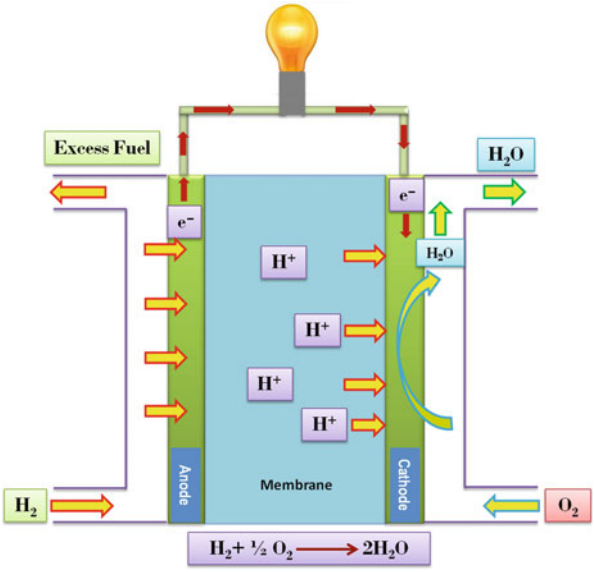

Fig. 22.2 Schematic depiction of PEMFC

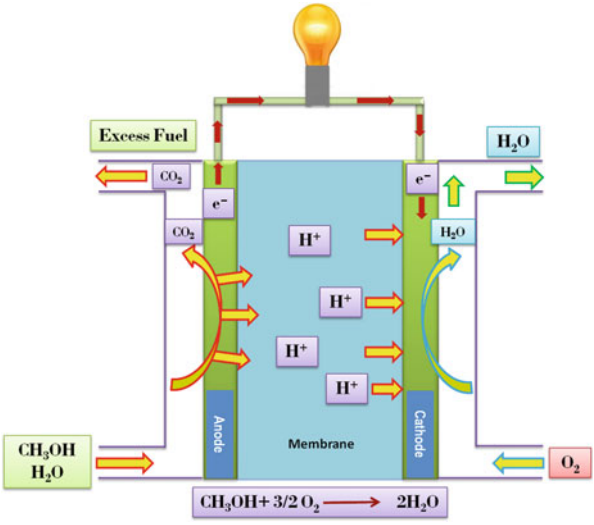

Fig. 22.3 Schematic depiction of DMFC

2 Development of Polymer Membranes for Fuel Cell Applications

The first polymer membrane developed for the Gemini space program by GE was based on the sulfonated polystyrene divinylbenzene copolymer, but high membrane cost and very short life span had limited its application. Nafion® (introduced by Dupont in 1972) is the most suitable and commercialized membrane till date with

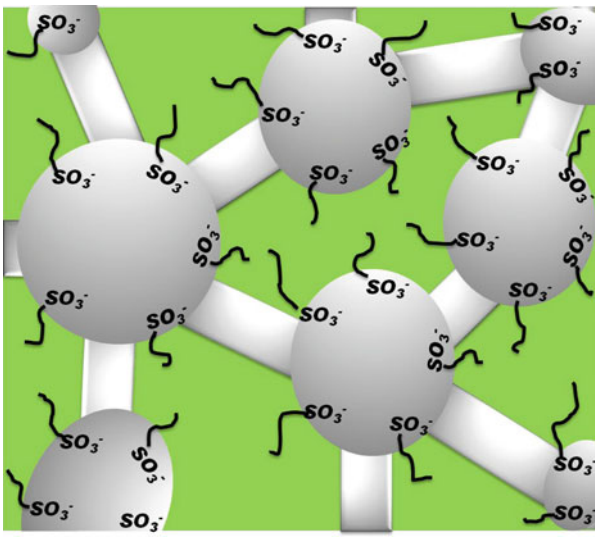

Fig. 22.4 Ion conduction channels present in Nafion under highly humidified conditions

a very high conductivity of 0.7–1.0 S cm^{-1} at room temperature and 100 % relative humidity (RH). The perfluorinated backbone in Nafion® provides strength to the membrane, whereas the sulfonic acid group provides the path for proton conduction. Different models (such as cluster network model [15], core-shell model [16, 17], local-order model [18–20], sandwich model [21], rod model [22], and parallel water channel model [23]) have been proposed based on small-angle X-ray scattering (SAXS), wide-angle X-ray diffraction studies, and solid-state NMR studies to describe the proton conduction mechanism in Nafion. The proposed models are still under investigation; however, all of the models suggest the presence of interconnected ion channels in Nafion® (Fig. 22.4). The $–SO_3H$ groups on the Nafion® backbone self-organize to form a hydrophilic water channel under highly humidified conditions, through which small ions can be easily transported. Under low hydration conditions (at low humidity and high temperature), the ionic clusters are disconnected from each other leading to inferior conductivity of Nafion [1, 7, 13]. PEMFCs operating above 100 °C are preferred over that operating at low temperature to overcome several disadvantages (like CO catalyst poisoning and heat and water management) associated with the later [1, 6, 7, 24]. Inferior proton conductivity of Nafion at high temperature and low humidity has prompted towards the development of new polymer membranes such as polyethersulfone (PES) [25, 26], polyetheretherketone (PEEK) [27–30], polyimide (PI) [31–33], polybenzimidazole (PBI) [34–41], polystyrene-acrylonitrile (SAN) [42, 43], and polyvinylidene fluoride (PVDF) [44–46] to meet the U. S. Department of Energy (DOE) targets [47, 48].

The membrane suitable for DMFC should possess acceptable proton conductivity along with good barrier property to prevent methanol crossover and water transport (by diffusion or electroosmotic drag). Methanol diffusion through the

membrane in DMFC from the anode to the cathode imparts reduced fuel cell performance and voltage efficiency. Sulfonation of polymer in both PEMFC and DMFC improves the proton conductivity and water uptake of the membranes [49–52]. The degree of sulfonation is also directly proportional to the proton conductivity of the membrane. However, high degree of sulfonation leads to unnecessary swelling of the membrane upon hydration and decreases the mechanical stability. This makes the membrane unsuitable for MEA fabrication [1, 7, 53, 54]. These problems can partly be overcome by incorporating inorganic fillers into the polymer matrix due to their reinforcing nature and high barrier property towards gases and solvents.

Several inorganic nanomaterials, such as layered silicates (clay) [1, 7, 55–57], silica [58–64], polyhedral oligomeric silsesquioxane [65, 66], titanium dioxide [56, 67, 68], zirconium dioxide [69, 70], heteropolyacids [27, 71], carbon nanotubes [72–76], and graphene oxides [77, 78], are being used for the fabrication of organic–inorganic hybrid membranes for both PEMFC and DMFC applications. Layered silicates are known for their high barrier property towards gases and solvents due to their unique layered and platelet type structure [79]. In addition, they can improve the mechanical properties of their respective nanocomposites due to their reinforcing nature [79–82]. The high hydrophilicity of clay provides additional benefit to improve the proton conductivity of the nanocomposites compared to the virgin membranes [1].

3 Proton Conduction Mechanism in Membrane

The proton conduction through polymer membranes basically follows two types of mechanisms: vehicle and Grotthus mechanism. The proton requires a vehicle or carrier in vehicle mechanism, while it moves from the anode to the cathode through a network of hydrogen bond in Grotthus mechanism. An artistic presentation of the two mechanisms has been proposed by Kreuer (Fig. 22.5) [83]. The membrane

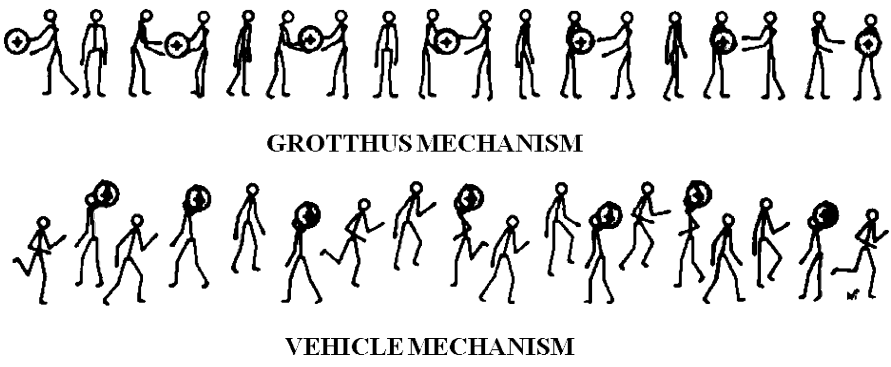

Fig. 22.5 Schematic representation of the phenomenon involved in proton conduction mechanism (see Ref. [83])

conductivity can be further enhanced by the addition of hygroscopic inorganic nanofillers such as silica or clay to the membrane, addition of proton-conducting fillers such as heteropoly acids, modification of the polymer surface with proton-conducting groups like $–SO_3H$ and $–PO_3H$ groups, and doping of the basic polymers (such as polybenzimidazole) with phosphoric acids. Surface modification of inorganic fillers with modifiers end capped with proton-conducting groups can further improve the proton conductivity.

4 Surface Modifications of Nanoclays

Layered silicates are known to provide superior properties to their respective polymer-based nanocomposites in their delaminated (exfoliated) state. In order to increase the compatibility between the organic polymer and inorganic silicates and also to increase the interlayer gallery spacing, surfaces of the silicates are generally modified with organic modifiers [79–82]. Despite the surface modifications, it is difficult to achieve complete exfoliation of clay in the polymer matrix. Generally, a combination of exfoliated and intercalated morphology of layered silicates in polymer matrix is most frequently encountered [79–82].

Inorganic nanoclays are nonconducting in nature towards protons. Hence, nanoclays dispersed in the polymer matrix act as barrier for the proton migration from anode to cathode. Hence, surface modifications of nanoclays with proton-conducting groups can be beneficial for improved proton conductivities of the nanocomposites compared to the virgin polymer and the composites containing unmodified clays [1, 7].

Surface modifications of nanoclays are being carried out in three ways (ionic, covalent, and plasma treatment) [1]. Ionic modifications of nanoclays are performed in two ways (acid activation and conventional ion exchange with alkyl ammonium ions) by the replacement of exchangeable Na^+ ions present in the interlayer gallery spacing of nanoclays. The covalent modification of nanoclays involves the reaction between the –OH groups present on the surface of the nanoclays with alkyl silanes. However, plasma treatment involves the modifiers end capped with vinyl groups. In order to improve the proton conductivity of the nanoclays, surface modifiers containing $–SO_3H$ and $–PO_3H$ groups are being used for the modifications of nanoclays. Different modifiers used for clay modifications via ionic modification technique include sulfanilic acid (SA), dimethyldioctadecylammonium chloride (DMDOC), chitosan, dodecylammonium chloride, and cetyltrimethylammonium chloride (CTAC) [84–89]. Similarly, the modifiers used for the modification of clay by covalent modification technique are 2-acrylamido-2-methyl-1-propanesulfonic acid (AMPS); 3-mercaptopropyltrimethoxysilane (3-MPTMS); 1,3-propane sultone; 1,4-butane sultone; 1,2,2-trifluoro-hydroxy-trifluomethylethane sulfonic acid sultone (FMES); glycidoxypropyl triethoxysilane (GPTES); 3-2-imidazolin-1-yl-propyltrimethoxysilane and amino-propyl trimethoxysilane (APTMS); (3-aminopropyl) triethoxysilane (APS); and imidazolin-1-yl-glycidylpropyltriethoxysilane (IGPTES) [90–92].

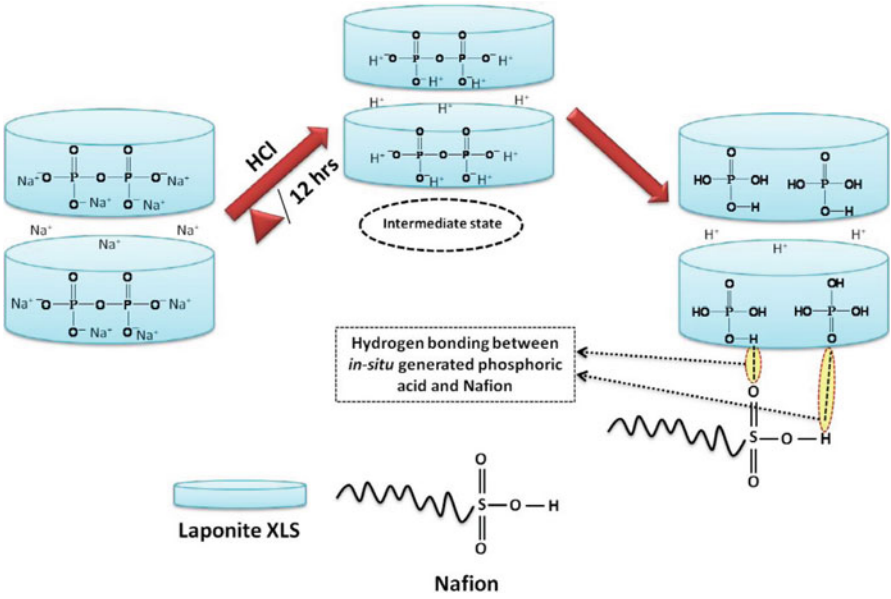

Fig. 22.6 Acid activation of Laponite XLS nanoclay in dilute hydrochloric acid (see Ref. [101])

However, p-styrene sodium sulfonate and SO_2 are being used as modifiers for the modification of clay by plasma treatment technique [93–96].

Acid activation of nanoclay leads to the replacement of Na^+ ions from the interlayer gallery of the nanoclays [97–100]. The ionic mobilities of the H^+ ions are higher than that of the Na^+ ions owing to the lower atomic size of H^+ ions compared to that of the Na^+ ions. Hence, the proton conductivity of the acid-activated clay is expected to be higher than the unmodified clay. Mishra et al. used similar technique for the modification of Laponite XLS (peptized Laponite clay) [101]. Interestingly, in this case, the peptizer ($Na_4P_2O_7$) present on the clay surface hydrolyzed to generate H_3PO_4 (in situ), along with the conventional replacement of Na^+ ions by H^+ ions from the interlayer gallery of the clay (Fig. 22.6). It is worth mentioning here that H_3PO_4 is well known for its high proton conductivity [1, 6].

5 Fabrication of Polymer-Clay Nanocomposite Membranes for Fuel Cell Applications

Different solvents were used for the preparation of Nafion-clay nanocomposite membranes comprised of unmodified, modified, and acid-activated clays [85, 92, 102, 103]. Nafion® 112 solution in ethanol-water (50:50 by weight) was heated at 250 °C in a reactor for 24 h, cooled, and then neutralized by the dropwise addition of 0.1 M NaOH solution. The resulting perfluorosulfonic acid (PFSA) crystals were

ball-milled to prepare a white powder. The nanoclay was added to a solution of the PFSA powder in DMF, followed by mixing, sonication, and solvent evaporation to prepare the nanocomposite membrane [56]. Xiuchong et al. mixed modified MMT in 5 % Nafion® dispersion and kept the solution in an autoclave at 150 °C for 4 h with rapid stirring and subsequently evaporated the solvent at 100 °C [104]. Fatyeyeva et al. [105, 106] mixed modified Laponite with polyethylene glycol (PEG) 1500 and water with continuous stirring and ultrasonication. The mixture was then freeze dried to obtain exfoliated clay mixture in PEG. Recast Nafion (from 20 % Nafion® dispersion) was added to the DMF dispersion of the aforementioned clay mixture. The solvent was evaporated in a controlled heating condition to prepare the nanocomposite membrane. However, Bébin et al. added recast Nafion® directly to a 15 % (w/v) DMF-clay suspension to prepare the Nafion®-clay nanocomposite membrane [94].

The polymers like sulfonated polyether ether ketone (SPEEK), polyamide (PAM), sulfonated polysulfone (SPSU), and polystyrene ethylene butylene polystyrene (PSEBS) are soluble in polar solvents like dimethyl acetamide (DMAc), dimethyl formamide (DMF), N-methyl pyrolidone (NMP), and tetrahydrofurane (THF). Hence, the nanoclays and the polymer were dispersed in these solvents to prepare the respective nanocomposites [93, 107–109]. Similarly, water was chosen for the water soluble polymer like poly(vinyl alcohol) (PVOH). The as-prepared PVOH-clay membrane was immersed in HPW solution in water (0.66 wt%) to improve the proton conductivity [110].

6 Effects of Modifications on the Physical Properties of the Hybrid Membranes

As already mentioned earlier, modifications of nanoclays are necessary to improve the compatibility between the organic polymer and the inorganic nanoclays. However, the improvements in the physical properties like thermomechanical, barrier property, water uptake, proton conductivity, and the cell performance of the hybrid membranes mainly depend on the types of modifier to the nanoclay and the degree of dispersion of the nanoclays in the polymer matrix.

6.1 Permeability

Impermeable nanoclay layers in polymer matrix mandate a tortuous zigzag diffusion pathway for solvents and gases to transverse the membrane (Fig. 22.7). Hence, the permeability of the resulting polymer-clay nanocomposites lowers down compared to the virgin polymer. This behavior of the polymer-clay nanocomposite membranes enhances the fuel cell performance by reducing the fuel crossover.

The methanol permeability (defined as the product of diffusivity and solubility) of recast Nafion® was nearly 2.3×10^{-6} cm^2/s compared to that of 1.6×10^{-7} cm^2/s for Nafion®/MMT nanocomposite membranes containing 1 wt% MMT with a nominal

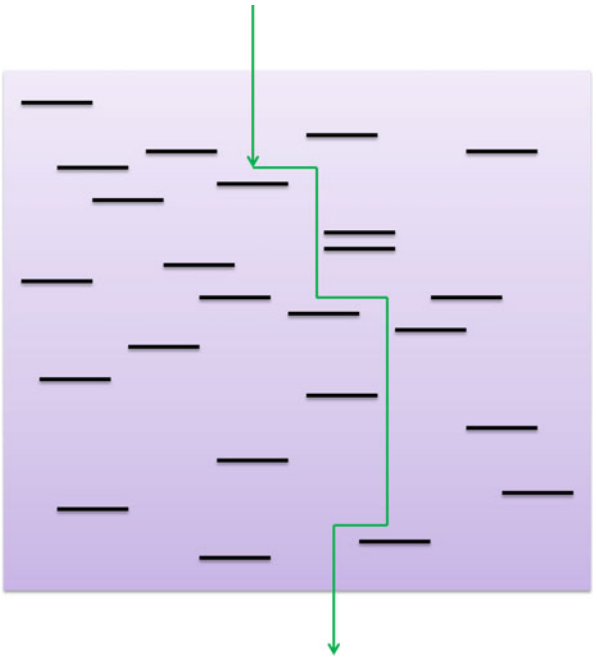

Fig. 22.7 Schematic depiction of the polymer-clay nanocomposite representing the barrier effect of nanoclay

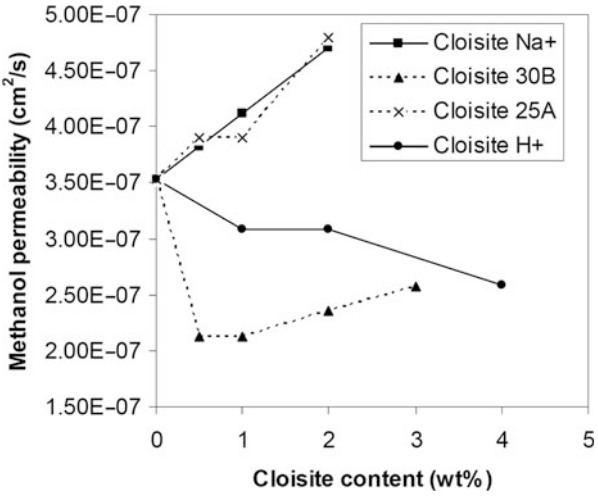

Fig. 22.8 Methanol permeability of Nafion-clay nanocomposites comprised of nanoclays with different counter ions (see Ref. [113])

thickness of 50 μm [111, 112]. Addition of sulfonated MMT and Cloisite 30B to Nafion reduced the methanol and water permeability relative to the virgin Nafion due nm m to their well-dispersed morphology in Nafion [89, 113]. However, poor polymer-filler interactions resulting in the void formation in the polymer-filler interface and inferior dispersion of unmodified MMT in Nafion reduced the barrier

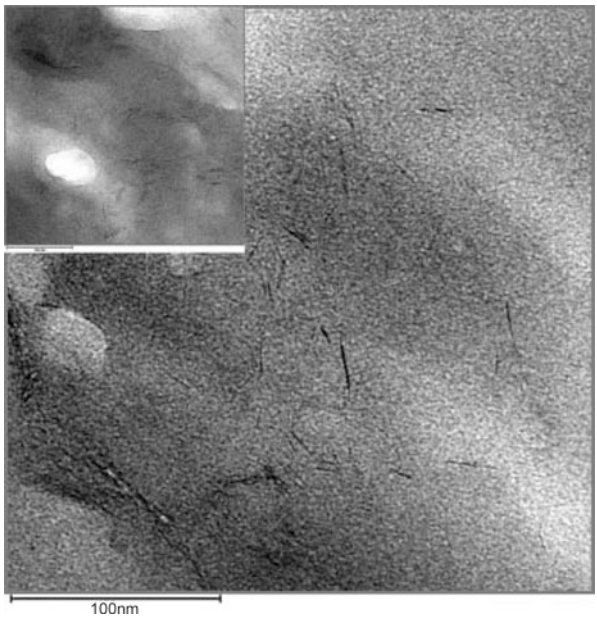

Fig. 22.9 TEM images of SPAS-clay nanocomposite containing 3 wt% Laponite (*inset* shows its low-magnification TEM image, see Ref. [115])

effect of Nafion-based composite towards methanol compared to the virgin Nafion (Fig. 22.8) [113].

The methanol permeability of SPEEK is lower than that of Nafion 115 due to the difference in the microstructure between these two varieties of membranes. Presence of small hydrophilic-hydrophobic interaction, low flexibility of the polymer backbone, and highly branched structure of SPEEK renders narrow proton conduction channels which perplex the methanol transport through the membrane. The methanol permeability further lowers down with the addition of OMMT due to the barrier effect of the nanosized dispersion of OMMT [87]. SPEEK (degree of sulfonation 67 %) possesses the permeabilities of 18 and 127 cm^2/s towards methanol and water, respectively. Addition of unmodified and modified Laponite (modified with imidazoleglycidoxypropyl triethoxysilane) resulted in a decrease in the permeability of the nanocomposites compared to the virgin SPEEK. Methanol and water permeabilities of SPEEK-modified Laponite composite membranes containing 20 wt% clay were reported to be 7 and 74 cm^2/s, respectively, while the corresponding values of the analogous membranes prepared with unmodified Laponite were noted to be 11 and 79 cm^2/s, respectively. This behavior was due to the higher compatibility of the SPEEK with the modified clay compared to that of the unmodified clay [114].

Highly exfoliated structure of Laponite in SPAS matrix (Fig. 22.9) resulted in a decrease in the permeability of the resulting nanocomposite membranes compared to the virgin SPAS. The methanol permeability of the SPAS-clay

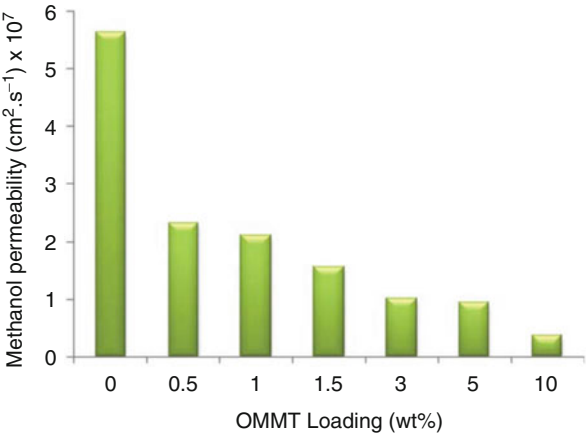

Fig. 22.10 Effect of nanoclay loading on the methanol permeability of the PBI-clay nanocomposite (see Ref. [116])

nanocomposite and SPAS was found to be 1.55×10^{-7} and 3.47×10^{-6} cm^2/s, respectively [115]. A drastic decrease in the methanol permeability of the PBI-MMT nanocomposites was also noted with the increase in the clay content (Fig. 22.10) [116]. However, the methanol permeability of the PVOH-clay nanocomposites was noted to increase with the clay content beyond 7 wt% clay content due to the increased aggregation of clays (or reduced number of individual sheets) [110]. Hence, exfoliated clay morphology and better polymer-clay interaction can reduce the permeability of both water and methanol to a significant extent and vice versa. Types of modifier to the clay do not play a significant role in altering the permeability of the nanocomposites.

6.2 Mechanical Properties

The reinforcing nature of nanoclays enhances the mechanical properties of the nanocomposites compared to the virgin membranes [55, 109]. The tensile strength (TS) and elongation at break (EB) for extruded Nafion® membrane were approximately 30 MPa and 200 %, respectively. Addition of 3 wt% of MMT to Nafion increased the TS and EB by 35 % and by twofold, respectively, compared to the virgin Nafion (Fig. 22.11a,b) [111]. In a similar study, SPAS-clay nanocomposite inferred a significant improvement in the mechanical strength compared to the virgin SPAS [115]. This is possible due to high degree of dispersion of nanoclays in the polymer matrices (Fig. 22.9). The storage modulus (E′) of the virgin PVOH and PVOH-MMT nanocomposite containing 5 and 10 wt% clay was noted to be 1,360, 4,010, and 5,430 MPa, respectively [110]. Increase in the clay content had a positive influence in improving the mechanical properties of the nanocomposites up to a certain amounts of clay content beyond which the mechanical properties started deteriorating [110]. This was ascribed to the inferior clay dispersion in the polymer matrix at higher clay content.

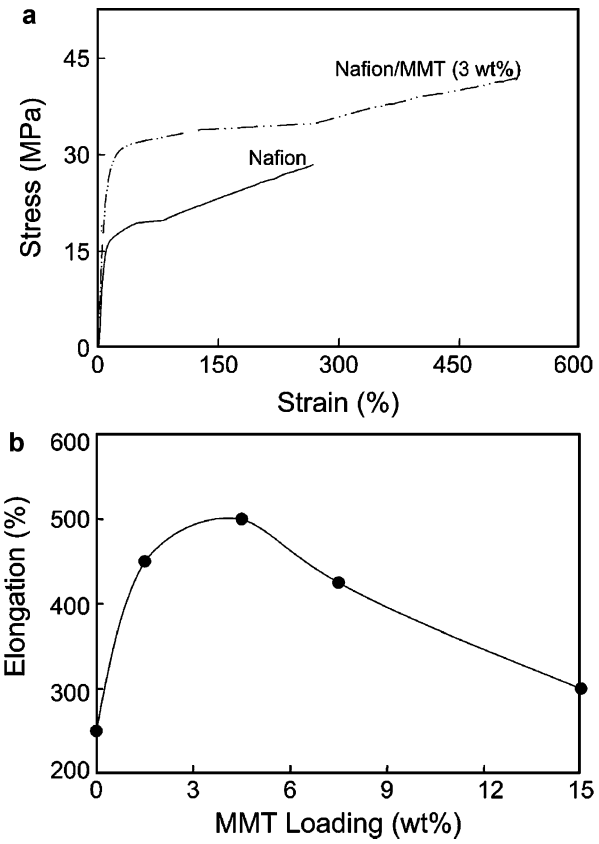

Fig. 22.11 (a) Stress-strain curve and (b) elongation of Nafion-MMT nanocomposite (see Ref. [111])

6.3 Thermal Stability

Three stages of degradation are generally observed for Nafion®. The weight loss up to 300 °C corresponds to the loss of water molecules, whereas the weight loss commencing at 350 °C and between 400 °C and 520 °C corresponds to the decomposition of $–SO_3H$ groups and oxidative degradation of the teflonic polymer backbone, respectively [61]. Addition of modified MMT to Nafion® resulted in an increase in the thermal stability of the nanocomposite membrane compared to that of the virgin Nafion® (Fig. 22.12) [102, 111]. This can be attributed to the strong interfacial bonding between the Nafion and the modified MMT. However, Song et al. reported an increase in the second degradation temperature of the Nafion-MMT nanocomposite despite similar onset degradation temperature to that of the virgin Nafion. The delayed weight loss of the nanocomposites compared to the virgin membranes is due to the fact that the nanodispersed nonconducting clays prevent faster heat transmission through the membrane [112].

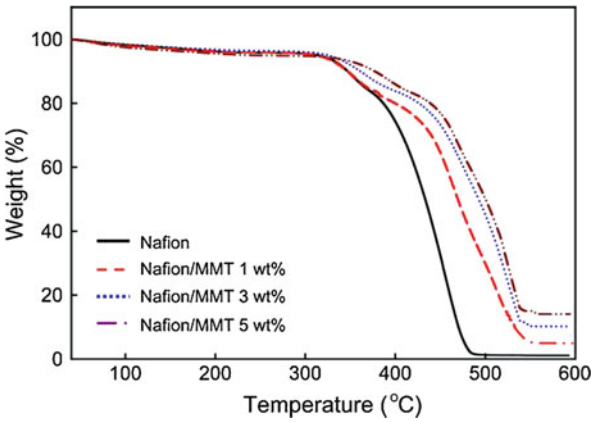

Fig. 22.12 TGA thermograms of Nafion-MMT nanocomposites (see Ref. [111])

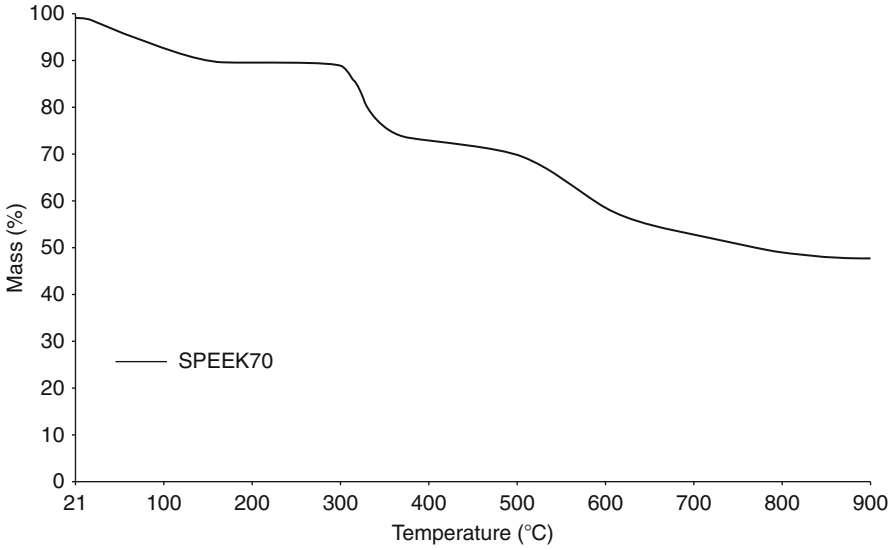

Fig. 22.13 TGA thermogram of SPEEK membrane (see Ref. [117])

A SPEEK membrane produces two degradation peaks at 300–400 °C and 550 °C, corresponding to the loss of $–SO_3H$ groups and main-chain degradation, respectively (Fig. 22.13). Addition of modified clay improved the thermal stability of the nanocomposite compared to that of the virgin SPEEK to a smaller extent [108, 117]. Similarly, the addition of MMT to the SPSEBS and PVOH enhanced the thermal stabilities of the respective nanocomposites compared to the virgin membranes [109, 110]. The increased thermal stabilities of the nanocomposite membranes are due to the high thermal stabilities of the

inorganic silicates. However, addition of PWA to PVOH-MMT composites reduced the initial degradation temperature of the nanocomposite membranes due to the catalytic effect on polymer dehydration [110].

6.4 Water Uptake

Water uptake of the membrane is an important parameter due to its assistance in the proton conduction of the membrane. It can be calculated using the following equation:

$$\text{Water uptake} = \frac{W_t - W_d}{W_d} \times 100$$

where W_d is the dry weight of the membrane and W_t is the weight of the membrane after swelling at a particular temperature for 24 h. The water uptakes of various polymer membranes are summarized in Table 22.1.

The room temperature water uptake of Nafion® is ~33 %, and it increases with increased temperature. Addition of nanoclay to Nafion increases the water uptake of the composite membrane due to the hydrophilic nature of the nanoclays. Increasing the nanoclay content in Nafion further increases the water uptake of the composite membranes [92, 104]. Nafion-based composite membranes comprised of sulfonated Laponite RD and unmodified Laponite RD had shown the water uptake of 70 % and 87 %, respectively, compared to 50 % for the virgin Nafion® at 85 °C [94, 106]. In contrast, poor polymer-filler interaction between the Nafion and unmodified MMT lowered the water uptake of the Nafion®-unmodified MMT nanocomposite membrane compared to the virgin Nafion® (Fig. 22.14) [92, 112].

In the case of sulfonated polymers like SPEEK, sulfonated polyarylene sulfone (SPAS), and sulfonated polyether sulfone (SPES), degree of sulfonation (DS) of the polymer determines the water uptake values. SPPEK membranes with DS of 69.4 % and 85 % imparted water uptakes of 42 % and 91 %, respectively [60]. Presence of the hydrophilic groups (like $–SO_3H$ groups) on the modifier to the clay improved the water uptake of the resulting nanocomposite membranes. In contrast, highly hydrophobic modifier (dimethyldioctadecylammonium chloride) to the clay reduced the water uptake of the nanocomposite [112, 117]. Gaowen et al. observed constant water uptake of the nanocomposites irrespective of the temperature due to the matrix stiffening effect of nanoclays on the SPEEK matrix, which restricted the membrane from further swelling at high temperature [87].

Interestingly, the sulfonated PVOH-unmodified MMT nanocomposites imparted low water uptake at low clay content, with a gradual increase of the same at high clay content (Fig. 22.15). This behavior is possibly due to the low affinity of unmodified MMT towards water compared to the sulfonated PVOH along with reduced number of hydrophilic groups (due to the H-bonding between the surface –OH groups of MMT and $–SO_3H$ groups of sulfonated PVOH) [118]. On the contrary, lower water affinity of MMT compared to PWA reduced the water uptake of the PVA-PWA-MMT composite compared to that of the PVA-PWA composite membranes [110].

Table 22.1 Water uptake and cell performance of different membranes

Type of membrane	Water uptake (%)	Operating temperature (°C)	Methanol solution feed	Cell voltage (V)	Current density (mA cm^{-2})	References
Recast Nafion®	50.0	80	–	0.6	600	[94]
Nafion®-10 wt% Laponite	87.0		–		–	
Nafion®-10 wt% sulfonated Laponite	70.0		–		720	
Nafion®	13.5	60	–	60	550	[92]
Nafion®-5 wt% H^+ MMT	13.1		–		–	
Nafion®-5 wt% sulfonated MMT	20.1		–		800	
SPEEK	100	60	–	0.6	80	[108]
SPEEK-10 wt% Laponite	30		–		370	
Nafion	–	40	–	0.2	244	[89]
Nafion-5 % sulfonated MMT	–		–		336	
Nafion-10 % sulfonated MMT	–		–	0.2	286	[89]
Nafion 117	–	–	1 M	0.2	420	[91]
Nafion-3 wt% sulfonated MMT		–			460	
Nafion 117		–	5 M	0.2	210	
Nafion-3 wt% sulfonated MMT		–			390	
SPEEK	–	60	–	0.6	80	[108]
SPEEK-10 wt% Laponite clay	–		–		370	
SPEEK	47.4	80	–	–	–	[100]
SPEEK-5 wt% sulfonated clay	42.2	25	–	–	–	
SPEEK-5 wt% sulfonated clay	58.0	80	–	–	–	

6.5 Proton Conductivity

The proton conductivity of the virgin Nafion® at room temperature and at 100 % RH varies from 0.07 to 0.1 S cm^{-1}. The proton conductivities of the Nafion-clay nanocomposites are highly dependent on the degree of dispersion and types of surface modifier. Improved proton conductivity of the nanocomposites compared to the virgin membrane is mainly due to the high hydrophilicity of the nanoclays which improves the water retention property of both the nanocomposite membranes. This trend remains unchanged even upon UV irradiation of the

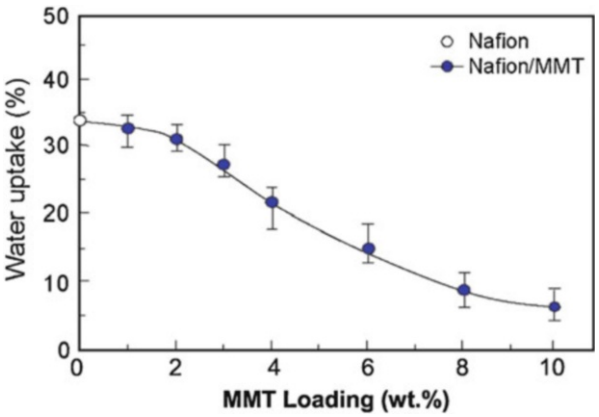

Fig. 22.14 Effect of MMT content on the water uptake behavior of Nafion-based composite membranes (see Ref. [112])

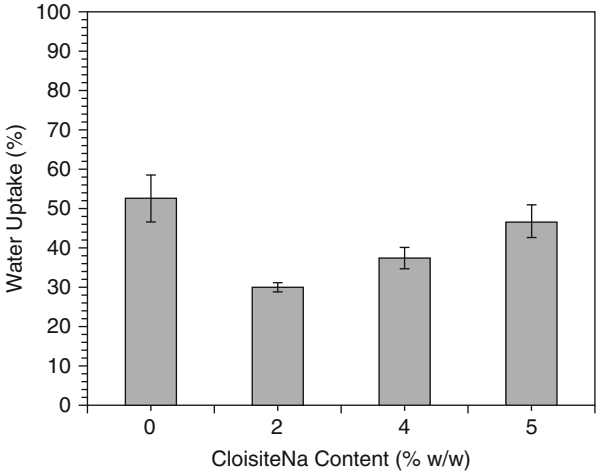

Fig. 22.15 Effect of unmodified MMT content on the water uptake behavior of sulfonated PVA (see Ref. [118])

nanocomposites and the virgin Nafion [104]. A comparative study between the nanocomposites containing MMT with different counter ions (H^+, Na^+, and ammonium counter ions) showed a highest conductivity with the acid-activated MMT (H^+ counter ion) compared to MMT having Na^+ and ammonium counter ions due to the ease in mobility of the smaller counter ions (H^+ ion) (Fig. 22.16) [113]. Sulfonation of the nanoclay surface was also noted to increase the proton conductivity of the resulting membrane compared to the virgin Nafion and Nafion®-unmodified Laponite nanocomposite due to the presence of the highly proton-conducting $–SO_3H$ group on the clay surface [94]. A novel technique was used by Mishra et al. for the preparation of Nafion-Laponite XLS nanocomposite membranes. In this case, the proton conductivity of the nanocomposites was significantly enhanced due to the presence of in situ generated H_3PO_4 (resulting from the acid activation of Laponite XLS). The proton conductivity of the virgin

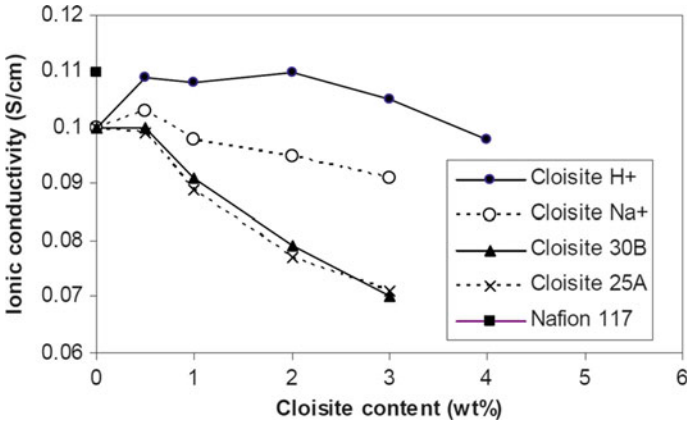

Fig. 22.16 Proton conductivities of Nafion-clay nanocomposites containing clay with different counter ions (see Ref. [113])

Nafion and the nanocomposite membrane containing 3 wt% of acid-activated Laponite were noted to be 0.14 and 0.27 S cm^{-1}, respectively, at 110 °C and 100 % RH [101].

In contrast to the above results, addition of the chitosan-modified MMT to Nafion resulted in a decrease in the proton conductivity with increasing clay contents [85]. The low conductivities of the Nafion-clay nanocomposites arise mainly due to the aggregated morphology of the clay or the presence of the hydrophobic modifier [111, 112]. Inferior clay dispersions in the polymer matrix lead to decreased conductivity of the nanocomposites even upon sulfonation of the clay surface [89].

In a similar study, SPEEK-clay nanocomposites revealed increased proton conductivities up to 10 wt% clay contents. However, further increase in the clay content was detrimental to the conductivity of the nanocomposites due to increased degree of obstacles for the proton mobility [114]. Modifiers to the clay which is indirectly related to the degree of dispersion of clay in the polymer matrix play a vital role in increasing or decreasing the proton conductivity. Hence, despite the presence of the proton-conducting groups like $–SO_3H$, SPEEK-clay nanocomposite based on SA-modified clay was lower than the virgin SPEEK, while the composite based on DMDOC-modified clay was higher than the virgin SPEEK (Fig. 22.17) [117]. The reduction in proton conductivity is mainly due to the blockage in the proton conduction channels created by the nonconducting nature of modifier or the aggregated clays [87, 107, 109, 116].

SPSU membrane with 72 % degree of sulfonation inferred proton conductivities of 0.09 and 0.17 S cm^{-1} at 30 °C and 85 °C, respectively, under 100 % RH [93]. The conductivity of the SPSU-sulfonated Laponite composite was enhanced by 25 % compared to that of the virgin SPSU due to increased sulfonated sites in the composite membranes.

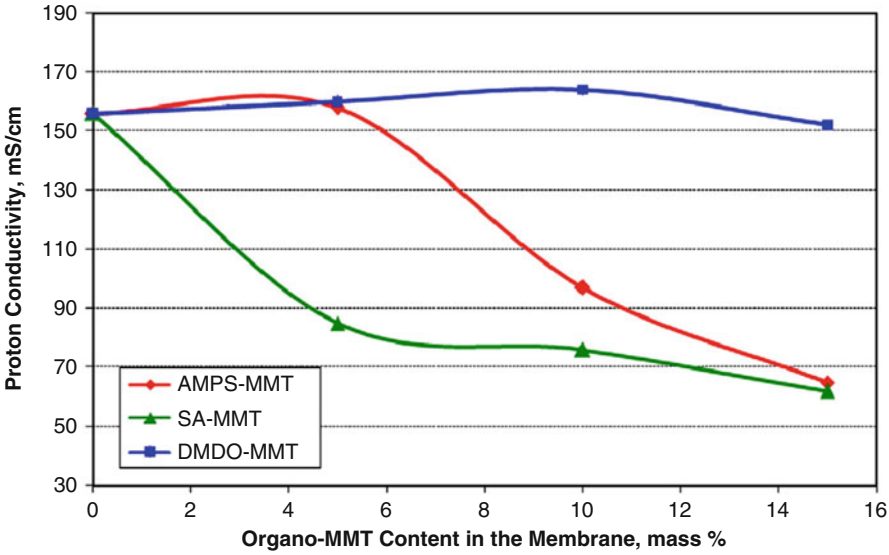

Fig. 22.17 Change in the proton conductivity of SPEEK-clay nanocomposite membranes with varying clay content and different types of clay (see Ref. [117])

Exfoliated morphology of Laponite in the SPAS matrix (Fig. 22.9) enhanced the conductivity of the nanocomposite than that of the virgin SPAS. The conductivity of the SPAS-clay nanocomposite varied from 0.099 to 0.187 S cm^{-1} within a temperature range of 20–70 °C [115]. PVOH membranes possess very low proton conductivity, and hence, it is doped with highly proton-conducting PWAs to improve the proton conductivities of the membranes. However, addition of PWA resulted in inferior mechanical properties of the nanocomposite membranes. PWA being highly conducting in nature compared to the clay, addition of MMT to PVOH-PWA composite resulted in a decrease in the conductivity of the PVOH-PWA-MMT composite compared to the PVOH-PWA composite [110]. In a similar study, addition of MMT (Cloisite 30B) to the highly conductive PAM-PS blend decreased the proton conductivity of the nanocomposite membrane compared to the PAM-PS blend [119]. Hence, despite the high hydrophilicity of nanoclays, degrees of dispersion of nanoclays in the polymer matrix play a vital role in improving the proton conductivity of the nanocomposites. The types of modifiers used for the clay modification can contribute to a very small extent in this regard.

6.6 Cell Performance

Cell performance study of the membranes can determine the suitability of the membrane for its end usage in fuel cell applications. Current densities and power

Table 22.2 Proton conductivities of different membranes

Type of membrane	Operating temperature (°C)	RH (%)	Proton conductivity (S cm^{-1})	References
Nafion®	90	98	0.200	[92]
Nafion®-5 wt% sulfonated MMT			0.160	
Nafion®-5 wt% protonated MMT			0.085	
Nafion®	95	98	0.064	[94]
Nafion®-10 wt% unmodified Laponite			0.065	
Nafion®-10 wt% sulfonated Laponite			0.080	
Nafion	110	100	0.136	[101]
Nafion-3 wt% acid-activated Laponite			0.270	
SPSU	90	100	0.170	[93]
SPSU-5 wt% sulfonated Laponite			0.220	
Nafion	25	100	0.086	[85]
Nafion-1 wt% chitosan-modified MMT			0.083	
Nafion-5 wt% chitosan-modified MMT			0.059	[85]
SPEEK	80	100	0.125	[100]
SPEEK-1 wt% sulfonated clay			0.166	
PVA	70	100	0.043	[120]
PVA-10 wt% MMT			0.032	

densities are the key factors which determine the cell performance of the membranes. The current density of the membrane is highly dependent on the temperature, humidity, and operating voltage. Table 22.2 summarizes the current densities of different clay-based nanocomposites under different experimental conditions.

In the case of PEMFC, hydrogen and oxygen gas are used as the fuel to determine the cell performance. The current density and the power density of the membranes are highly dependent on the thickness of the membrane. Hence, the maximum power densities of Nafion® NRE 212 (thickness 50.8 μm) and Nafion® NRE 211 (thickness 25.4 μm) were noted to be 0.97 and 1.27 W/cm^2, respectively, at 80 °C and 100 % RH (Fig. 22.18a, b) [106]. Addition of Laponite, modified by sultone and p-styrene sulfonic acid to Nafion, enhanced the maximum power densities to 1.36 and 1.41 W cm^{-2}, respectively. The current density of Nafion was noted to be 600 mA cm^{-2} at 0.6 V, 80 °C, and under highly humidified conditions. The current density of the nanocomposite was increased to 720 mA cm^{-2} under similar conditions, due to the incorporation of sulfonated Laponite to Nafion. The current densities of the nanocomposites were also noted to be dependent on the

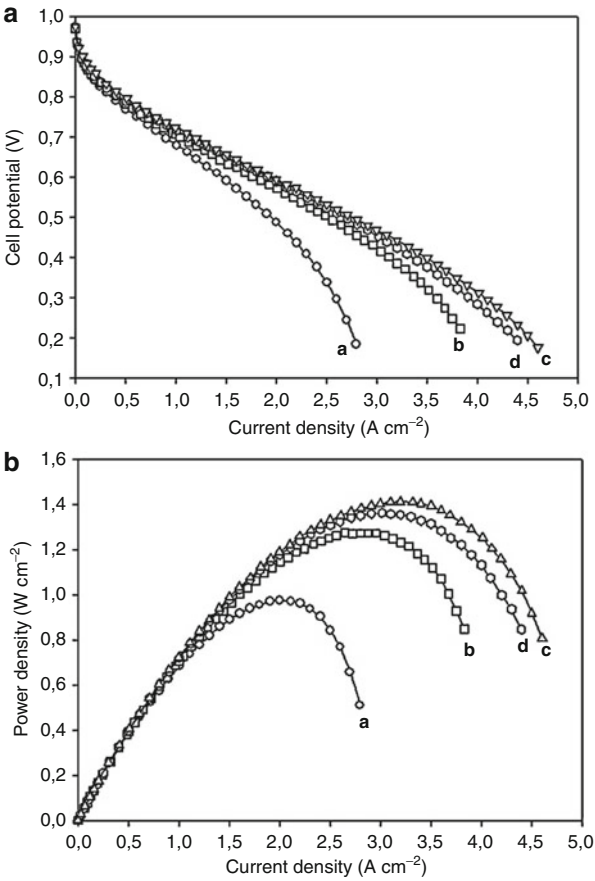

Fig. 22.18 Polarization curves (**a**) and power density curves (**b**) at 80 °C, total pressure of four absolute bars under dried H_2/O_2: *a* Nafion NRE212, *b* Nafion NRE211, *c* Nafion-Laponite-*p*-styrene sulfonic acid, *d* Nafion-Laponite-sultone membranes (see Ref. [95])

clay content. The current densities of Nafion-sulfonated MMT membranes increased with the clay content up to 5 wt% clay content (with a maximum value of 336 mA cm^{-2} at a potential of 0.2 V) and then deteriorated with further increase in the clay content due to increased aggregation of clay beyond 5 wt% clay content. The maximum power density of 67 mW cm^{-2} was also achieved for the composite membrane containing 5 wt% of sulfonated MMT (Fig. 22.19) [89].

In the case of DMFC, dilute methanol and oxygen gas are used as the fuel to determine the cell performance. Hence, the crossover current densities of the membranes are also dependent on the concentration of methanol. Hasani-Sadrabadi et al. reported the crossover current densities for Nafion 117 and the Nafion-clay nanocomposite to be 156 and 123 mA cm^{-2}, respectively, at 1 M methanol concentration and 518 and 320 mA cm^{-2}, respectively, at 5 M methanol concentration. Similarly, the limiting current densities for Nafion 117 and the Nafion-clay composite at the anode side were 530 and 555 mA cm^{-2}, respectively, at 1 M methanol concentration, whereas the values were 260 and 630 mA cm^{-2},

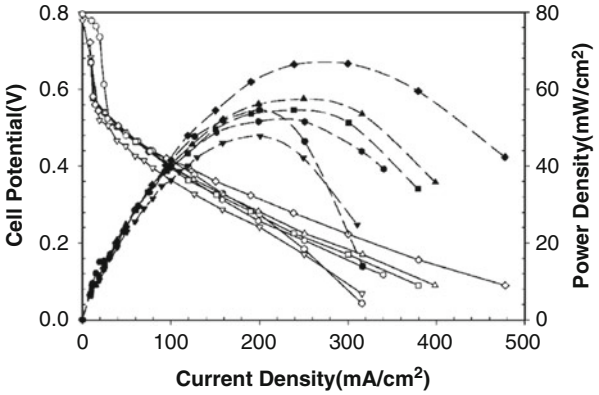

Fig. 22.19 Polarization curves for the MEA made with Nafion115 and composite membranes operated at 40 °C (2 M methanol/air flow rate): ● Nafion 115, ▼ Nafion-3 wt% unmodified MMT, ■ Nafion-3 wt% sulfonated MMT, ◆ Nafion-5 wt% sulfonated MMT, ▲ Nafion-10 wt% HSO3-MMT, ⬢ Nafion-15 wt% sulfonated MMT. The same symbols (but open ones) denote cell potentials for corresponding samples (see Ref. [89])

respectively, at 5 M methanol concentration. The higher open circuit voltage (OCV) values of the nanocomposite compared to the Nafion 117 indicated a drastic reduction in the methanol crossover from the anode to the cathode, which hampers the catalytic activity for oxygen reduction and also leads to the reduction in the fuel efficiency. Hence, addition of nanoclay to Nafion resulted in increased fuel cell efficiency, especially at high methanol concentration. The maximum power density of the Nafion 117 and the composites was noted to be 47 and 171 mW cm^{-2}, respectively, at 5 M methanol feed (Fig. 22.20) [85]. The DMFC cell performance study of SPAS-clay nanocomposite was found to be higher than the Nafion 115 membrane. The power densities of SPAS-clay nanocomposite were obtained to be 110, 145, and 191 mW cm^{-2} at 50 °C, 60 °C, and 70 °C, respectively, compared to those of 77, 119, and 142 mW cm^{-2} at 50 °C, 60 °C, and 70 °C, respectively, for Nafion 115. The increase in the operating temperature had also a positive influence in increasing the power density (Fig. 22.21 a, b) [115].

The current densities of the acid-doped PBI membrane, PBI-clay nanocomposite (3 wt% clay content), and Nafion 117 were noted to be 290, 260, and 351 mA cm^{-2} at 1 M methanol feed and 635, 723, and 420 mA cm^{-2} at 5 M methanol concentration, respectively, at a constant potential of 0.2 V. Similarly, the power densities of the acid-doped PBI membrane, PBI-clay nanocomposite (3 wt% clay content), and Nafion 117 were noted to be 59, 51, and 77 mW cm^{-2}, respectively, at a methanol concentration of 1 M and 130, 145, and 83 mW cm^{-2}, respectively, at a methanol concentration of 5 M and at a constant potential of 0.2 V [116]. The reason behind the decreased current density and power density of PBI-clay nanocomposite compared to the virgin PBI at 1 M methanol concentration and the reverse trend at 5 M methanol concentration is not known, and it has to be investigated further.

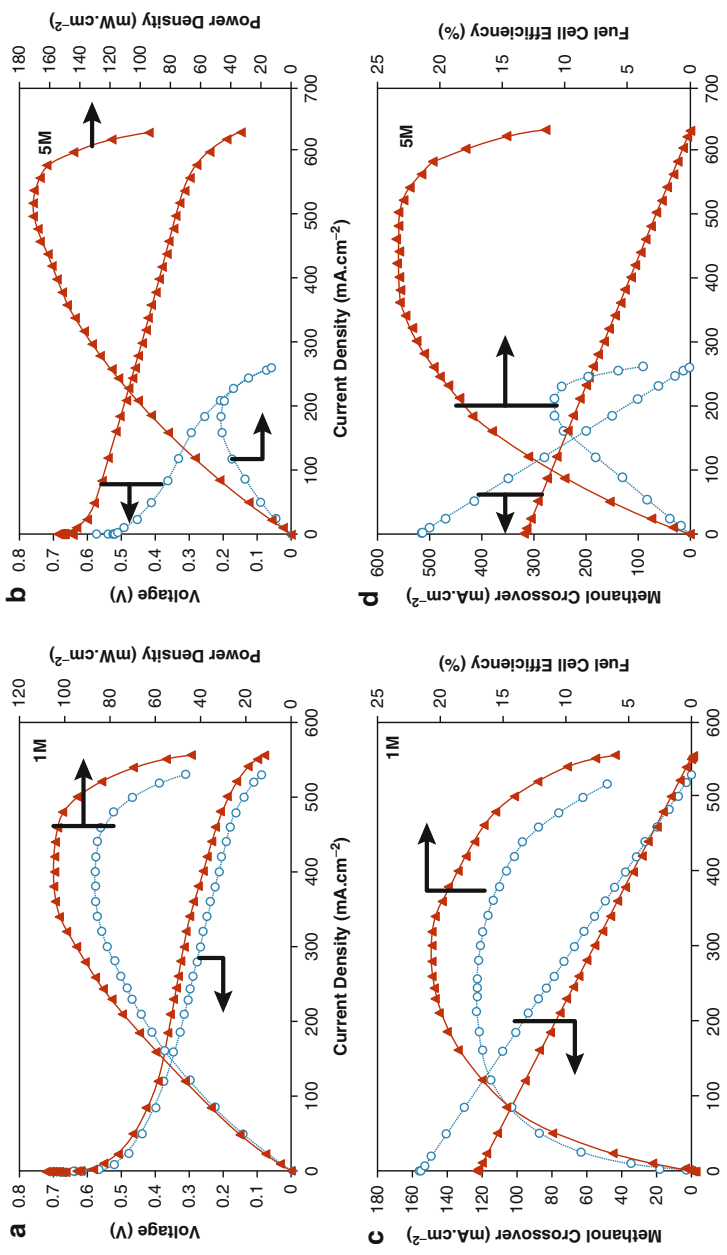

Fig. 22.20 Polarization curves of DMFC cells consisting of Nafion-2 wt% chitosan-modified MMT and Nafion 117, at (**a**) 1 M and (**b**) 5 M methanol solution at 70 °C. Methanol crossover and efficiency of the corresponding fuel cells at (**c**) 1 M and (**d**) 5 M methanol solution (see Ref. [85])

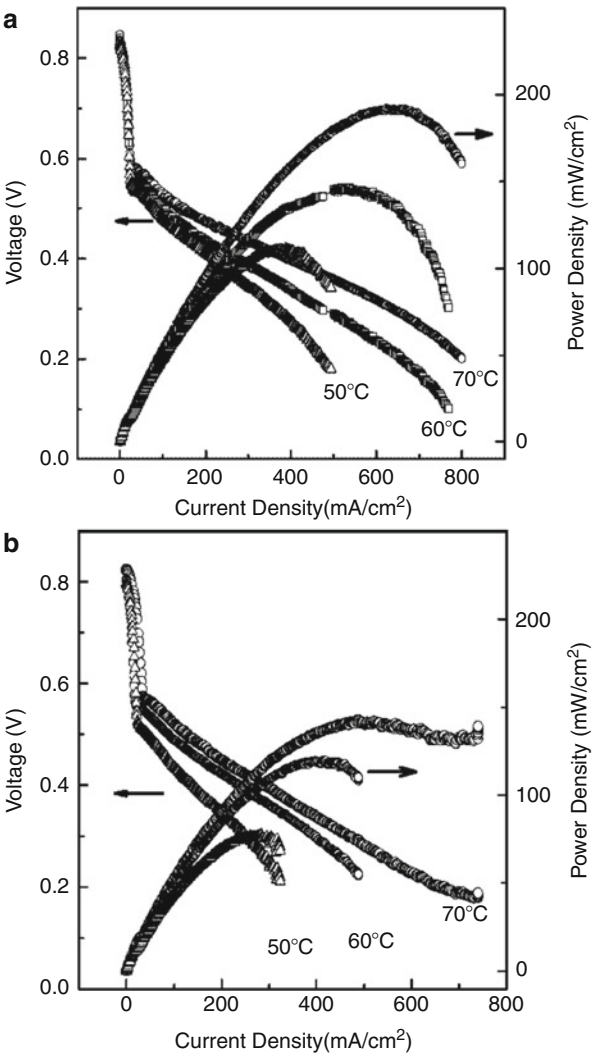

Fig. 22.21 Polarization curves of DMFC single cell test for SPAS-clay nanocomposite containing 3 wt% Laponite (**a**) and Nafion 115 (**b**) operated at different temperatures (see Ref. [115])

Thomassin et al. reported that the fuel cell performance of the membranes depends on the counter ion of the clay. Among three varieties of nanoclays studied, Cloisite 30B (with alkyl ammonium counterion), Cloisite Na^+ (with Na^+ counter ion), and Cloisite H^+ (with H^+ counter ion), Cloisite H^+ and Cloisite 30B provided the best and worst fuel cell performance, respectively. The current densities of Nafion 117 and Nafion-Cloisite H^+ were 100 and 60 mA cm^{-2}, respectively, at 80 °C and at a potential of 0.3 V (Fig. 22.22) [113].

It is worth mentioning here that the decrease in the proton conductivity of the nanocomposite does not confer similar trend in the fuel cell performance as well. Highly aggregated morphology of clay in the polymer matrix leads to the decrease

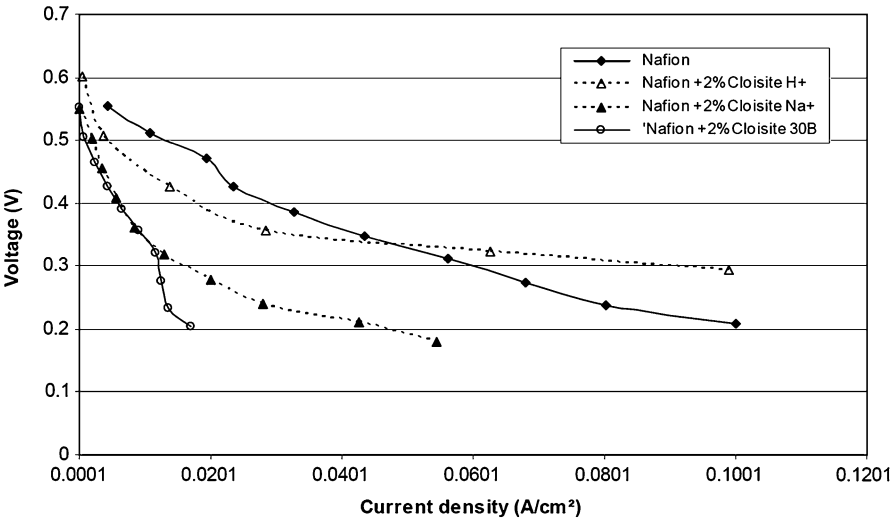

Fig. 22.22 Polarization curves for Nafion-clay nanocomposites at 80 °C (see Ref. [113])

in the water uptake and fuel cell performance [89, 92]. The operating temperature in PEMFC and methanol concentration in DMFC play vital role in improving the fuel cell performance.

7 Summary and Future Direction

The inferior proton conductivity of the Nafion membrane at high temperature and low humidity conditions along with the demerits associated with low-temperature fuel cells lead to the development of new membranes and techniques. Addition of nanoclay to the polymer is one of the techniques adopted to improve the operating temperature. This is due to the high hydrophilicity of the nanoclays and their water retention ability. In addition to that, the mechanical and thermal properties of the nanocomposites also increase with the incorporation of nanoclay to the polymer.

Improvements in all the physical properties of the clay-based nanocomposites are highly dependent on the degree of clay dispersion in the polymer matrix. Surface modifiers to the clay play a little role in improving the proton conductivity and the cell performance of the nanocomposites unless the clay platelets are well dispersed in the polymer matrix. However, in the case of the polymer-clay nanocomposites with well-dispersed clay, presence of $–SO_3H$ and $–PO_3H$ groups on the clay surface provided an additional path for the proton conduction and proved to be beneficial for high proton conductivity of the nanocomposites. High degree of clay dispersion is also responsible for the improvements in the thermomechanical property and water uptake of the nanocomposites along with the cell performance. Addition of clay to the polymer matrix leads to the slight increase

in the operating temperature due to the hydrophilic nature of clay. Despite tremendous efforts are being made to replace Nafion with other varieties of polymer membranes, no breakthrough has been achieved so far. Hence, plenty of research still has to be performed before the end usage of the clay-based nanocomposites. Highly conducting nature of ionic liquid can be beneficial for improved proton conductivity of the clay-based nanocomposites at low humidity conditions. The barrier effect of clay can prevent ionic liquid from leaching out of the membrane upon continuous usage. The plasticizing nature of the ionic liquid can also be counterbalanced by the reinforcing nature of the clay.

Acknowledgement This study was supported by the Converging Research Center Program (2013K000404) through the Ministry of Science, ICT & Future Planning and the Basic Science Research Program through the National Research Foundation (NRF) funded by the Ministry of Education of Korea (NRF-2013R1A1A2011608).

References

1. Mishra AK, Bose S, Kuila T, Kim NH, Lee JH (2012). Prog Polym Sci, 37:842–869
2. Grove WR (1839) Philos Mag 15:287–293
3. Grove WR (1839) Philos Mag 14:127–130
4. Grove WR (1842) Philos Mag 21:417–420
5. Couture G, Alaaeddine A, Boschet F, Améduri B (2011) Prog Polym Sci 36:1521–1557
6. Bose S, Kuila T, Nguyen TXH, Kim NH, Lau K-T, Lee JH (2011) Prog Polym Sci 36:813–843
7. Tripathi BP, Shahi VK (2011) Prog Polym Sci 36:945–979
8. Neburchilov V, Martin J, Wang H, Zhang J (2007) J Power Sources 169:221–238
9. Wasmus S, Kűver A (1999) Methanol oxidation and direct methanol fuel cells: a selective review. J Electroanal Chem 461:14–31
10. Couture G, Alaaeddine A, Boschet F, Améduri B (2011) Polymeric materials as anion-exchange membranes for alkaline fuel cells. Prog Polym Sci 36:1521–1557
11. Boudghene Stambouli A, Traversa E (2002) Solid oxide fuel cells (SOFCs): a review of an environmentally clean and efficient source of energy. Renewable Sustainable Energy Rev 6:433–455
12. Yang C, Costamagna P, Srinivasan S, Benziger J, Bocarsly AB (2001) J Power Sources 103:1–9
13. Souzy R, Ameduri B (2005) Prog Polym Sci 30:644–687
14. Rozière J, Jones DJ (2003) Annu Rev Mater Res 33:503–555
15. Hsu WY, Gierke TD (1983) J Membr Sci 13:307–326
16. Fujimura M, Hashimoto T, Kawai H (1982) Macromolecules 15:136–144
17. Fujimura M, Hashimoto T, Kawai H (1981) Macromolecules 14:1309–1315
18. Dreyfus B, Gebel G, Aldebert P, Pineri M, Escoubes M, Thomas M (1990) J Phys France 51:1341–1354
19. Gebel G, Lambard J (1997) Macromolecules 30:7914–7920
20. Gebel G (2000) Macromolecules 33:4850–4855
21. Haubold H-G, Vad T, Jungbluth H, Hiller P (2001) Electrochim Acta 46:1559–1563
22. Rubatat L, Rollet AL, Gebel G, Diat O (2002) Macromolecules 35:4050–4055
23. Schmidt-Rohr K, Chen Q (2008) Nat Mater 7:75–83
24. Li Q, He RH, Jensen JO, Bjerrum NJ (2003) Chem Mater 15:4896–4915
25. Harrison WL, Hickner MA, Kim YS, McGrath JE (2005) Fuel Cells 5:201–212
26. Miyatake K, Chikashige Y, Higuchi E, Watanabe M (2007) J Am Chem Soc 129:3879–3887

27. Zaidi SMJ, Mikhailenko SD, Robertson GP, Guiver MD, Kaliaguine S (2000) J Membr Sci 173:17–34
28. Liu B, Robertson GP, Kim DS, Guiver MD, Hu W, Jiang Z (2007) Macromolecules 40:1934–1944
29. Li L, Zhang J, Wang Y (2003) J Membr Sci 226:159–167
30. Zhang H, Fan X, Zhang J, Zhou Z (2008) Solid State Ion 179:1409–1412
31. Chen S, Yin Y, Kita H, Okamoto K (2007) J Polym Sci, Part A: Polym Chem 45:2797–2811
32. Miyatake K, Yasuda T, Hirai M, Nanasawa M, Watanabe M (2007) J Polym Sci, Part A: Polym Chem 45:157–163
33. Yin Y, Yamada O, Tanaka K, Okamoto K (2006) Polym J 38:197–219
34. Cho Y-H, Kim S-K, Kim T-H, Cho Y-H, Lim JW, Jung N, Yoon W-S, Lee J-C, Sung Y-E (2011) Electrochem Solid-State Lett 14:B38–B40
35. Zhang J, Tang Y, Song C, Zhang J (2007) J Power Sources 172:163–171
36. Ng F, Péron J, Jones DJ, Rozière J (2011) J Polym Sci, Part A: Polym Chem 49:2107–2117
37. Asensio JA, Sánchezab EM, Gómez-Romero P (2010) Chem Soc Rev 39:3210–3239
38. Li Q, He R, Jensen JO, Bjerrum NJ (2004) Fuel Cells 4:147–159
39. Asensio JA, Gómez-Romero P (2005) Fuel Cells 5:336–343
40. Bhadra S, Kim NH, Lee JH (2010) J Membr Sci 349:304–311
41. Bhadra S, Kim NH, Choi JS, Rhee KY, Lee JH (2010) J Power Sources 195:2470–2477
42. Lin B, Cheng S, Qiu L, Yan F, Shang S, Lu J (2010) Chem Mater 22:1807–1813
43. Diao H, Yan F, Qiu L, Lu J, Lu X, Lin B, Li Q, Shang S, Liu W, Liu J (2010) Macromolecules 43:6398–6405
44. Jones DJ, Rozière J (2008) Adv Polym Sci 215:219–264
45. Mustarelli P, Carollo A, Grandi S, Quartarone E, Tomasi C, Leonardi S, Magistris A (2007) Fuel Cells 7:441–446
46. Sel O, Soulès A, Améduri B, Boutevin B, Laberty-Robert C, Gebel G, Sanchez C (2010) Adv Funct Mater 20:1090–1098
47. Garland NL, Kopasz JP (2007) J Power Sources 172:94–99
48. Borup R, Meyers J, Pivovar B, Kim YS, Mukundan R, Garland N, Myers D, Wilson M, Garzon F, Wood D, Zelenay P, More K, Stroh K, Zawodzinski T, Boncella XJ, McGrath JE, Inaba M, Miyatake K, Hori M, Ota K, Ogumi Z, Miyata S, Nishikata A, Siroma Z, Uchimoto Y, Yasuda K, Kimijima K-i, Iwashita N (2007) Chem Rev 107:3904–3951
49. Park CH, Lee CH, Guiver MD, Lee YM (2011) Prog Polym Sci 36:1443–1498
50. Higashihara T, Matsumoto K, Ueda M (2009) Polymer 50:5341–5357
51. Iojoiu C, Maréchal M, Chabert F (2005) Fuel Cells 5:344–354
52. Jones DJ, Rozière J (2001) J Membr Sci 185:41–58
53. Hickner MA, Ghassemi H, Kim YS, Einsla BR, McGrath JE (2004) Chem Rev 104:4587–4612
54. Kerres J, Zhang W, Cui W (1998) J Polym Sci, Part A: Polym Chem 36:1441–1448
55. Xing D, He G, Hou Z, Ming P, Song S (2011) Int J Hydrogen Energy 36:2177–2183
56. Mura F, Silva RF, Pozio A (2007) Electrochim Acta 52:5824–5828
57. Felice C, Qu D (2011) Ind Eng Chem Res 50:721–727
58. Zou H, Wu S, Shen J (2008) Chem Rev 108:3893–3957
59. Durand N, Gaveau P, Silly G, Améduri B, Boutevin B (2011) Macromolecules 44:6249–6257
60. Reinholdt MX, Kaliaguine S (2010) Langmuir 26:11184–11195
61. Gnana Kumar G, Kima AR, Nahma KS, Elizabeth R (2009) Int J Hydrogen Energy 34:9788–9794
62. Jin YG, Qiao SZ, Xu ZP, Yan Z, Huang Y, Diniz da Costa JC, Lu GQ (2009) J Mater Chem 19:2363–2372
63. Jin YG, Qiao SZ, Xu ZP, Diniz da Costa JC, Lu GQ (2009) J Phys Chem C 113:3157–3163
64. Choi Y, Kim Y, Kim HK, Lee JS (2010) J Membr Sci 357:199–205
65. Choi J, Lee KM, Wycisk R, Pintauro PN, Mather PT (2010) J Electrochem Soc 157: B914–B919
66. Chhabra P, Choudhary V (2010) J Appl Polym Sci 118:3013–3023

67. Zhengbang W, Haolin T, Mu P (2011) J Membr Sci 369:250–257
68. Di Vona ML, Sgreccia E, Donnadio A, Casciola M, Chailan JF, Auer G, Knauth P (2011) J Membr Sci 369:536–544
69. Aparicio M, Klein LC (2005) J Electrochem Soc 152:A493–A496
70. Park KT, Jung UH, Choi DW, Chun K, Lee HM, Kim SH (2008) J Power Sources 177:247–253
71. Shao Z-G, Xu H, Li M, Hsing I-M (2006) Solid State Ion 177:779–785
72. Tripathi BP, Schieda M, Shahi VK, Nunes SP (2011) J Power Sources 196:911–919
73. Kannan R, Kakade BA, Pillai VK (2008) Angew Chem Int Ed 47:2653–2656
74. Thomassin J-M, Kollar J, Caldarella G, Germain A, Jérôme R, Detrembleur C (2007) J Membr Sci 303:252–257
75. Ijeri V, Cappelletto L, Bianco S, Tortello M, Spinelli P, Tresso E (2010) J Membr Sci 363:265–270
76. Kannan R, Aher PP, Palaniselvam T, Kurungot S, Kharul UK, Pillai VK (2010) J Phys Chem Lett 1:2109–2113
77. Zarrin H, Higgins D, Jun Y, Chen Z, Fowler M (2011) J Phys Chem C 115:20774–20781
78. Cao Y-C, Xu C, Wu X, Wang X, Xing L, Scott K (2011) J Power Sources 196:8377–8382
79. Ray SS, Okamoto M (2003) Prog Polym Sci 28:1539–1641
80. Mishra AK, Chattopadhyay S, Rajamohanan PR, Nando GB (2011) Polymer 52:1071–1083
81. Mishra AK, Nando GB, Chattopadhyay S (2008) J Polym Sci, Part B: Polym Phys 46:2341–2354
82. Mishra AK, Rajamohanan PR, Nando GB, Chattopadhyay S (2011) Adv Sci Lett 4:64–73
83. Kreuer K-D (1988) J Mol Struct 177:265–276
84. Zhang X (2007) J Electrochem Soc 154:B322–B326
85. Hasani-Sadrabadi MM, Dashtimoghadam E, Majedi FS, Kabiri K, Mokarram N, Solati-Hashjin M, Moaddel H (2010) Chem Commun 46:6500–6502
86. Ramírez-Salgado J (2007) Electrochim Acta 52:3766–3778
87. Gaowen Z, Zhentao Z (2005) J Membr Sci 261:107–113
88. Jung DH, Cho SY, Peck DH, Shin DR, Kim JS (2003) J Power Sources 118:205–211
89. Rhee CH, Kim HK, Chang H, Lee JS (2005) Chem Mater 17:1691–1697
90. Gosalawit R, Chirachanchai S, Shishatskiy S, Nunes SP (2008) J Membr Sci 323:337–346
91. Hasani-Sadrabadi MM, Dashtimoghadam E, Majedi FS, Kabiri K, Solati-Hashjin M, Moaddel H (2010) J Membr Sci 365:286–293
92. Kim Y, Choi Y, Kim HK, Lee JS (2010) J Power Sources 195:4653–4659
93. Buquet CL, Fatyeyeva K, Poncin-Epaillard F, Schaetzel P, Dargent E, Langevin D, Nguyena QT, Marais S (2010) J Membr Sci 351:1–10
94. Bébin P, Caravanier M, Galiano H (2006) J Membr Sci 278:35–42
95. Fatyeyeva K, Bigarré J, Blondel B, Galiano H, Gaud D, Lecardeur M, Poncin-Epaillard F (2011) J Membr Sci 366:33–42
96. Fatyeyeva K, Chappey C, Poncin-Epaillard F, Langevin D, Valleton J-M, Marais S (2011) J Membr Sci 369:155–166
97. Lee W, Kim H, Kim TK, Chang H (2007) J Membr Sci 292:29–34
98. Kim Y, Lee JS, Rhee CH, Kim HK, Chang H (2006) J Power Sources 162:180–185
99. Kim TK, Kang M, Choi YS, Kim HK, Lee W, Chang H, Seung D (2007) J Power Sources 165:1–8
100. Fu T, Cui Z, Zhong S, Shi Y, Zhao C, Zhang G, Shao K, Na H, Xing W (2008) J Power Sources 185:32–39
101. Mishra AK, Kuila T, Kim NH, Lee JH (2012) J Membr Sci 389:316–323
102. Zhang L, Xu J, Hou G, Tang H, Deng F (2007) J Colloid Interface Sci 311:38–44
103. Felice C, Ye S, Qu D (2010) Ind Eng Chem Res 49:1514–1519
104. Xiuchong H, Haolin T, Mu P (2008) J Appl Polym Sci 108:529–534
105. Fatyeyeva K, Chappey C, Poncin-Epaillard F, Langevin D, Valleton J-M, Marais S (2011) J Membr Sci 369:155–166

106. Fatyeyeva K, Bigarré J, Blondel B, Galiano H, Gaud D, Lecardeur M, Poncin-Epaillard F (2011) J Membr Sci 366:33–42
107. Hasani-Sadrabadi MM, Emami SH, Ghaffarian R, Moaddel H (2008) Energy Fuel 22:2539–2542
108. Chang J-H, Park JH, Park G-G, Kim C-S, Park OO (2003) J Power Sources 124:18–25
109. Swaminathan E, Dharmalingam S (2010) Int J Plast Technol 13:150–162
110. Thomassin J-M, Pagnoulle C, Caldarella G, Germain A, Jérôme R (2006) J Membr Sci 270:50–56
111. Song M-K, Park S-B, Kim Y-T, Kim K-H, Min S-K, Rhee H-W (2004) Electrochim Acta 50:639–643
112. Song M-K, Kim Y-M, Kim YT, Rhee H-W, Smirnova A, Sammes NM, Fenton JM (2006) J Electrochem Soc 153:A2239–A2244
113. Thomassin J-M, Pagnoulle C, Bizzari D, Caldarella G, Germain A, Jérôme R (2004) e-Polymers 018:1–13
114. Karthikeyan CS, Nunes SP, Prado LASA, Ponce ML, Silva H, Ruffmann B, Schulte K (2005) J Membr Sci 254:139–146
115. Choi YS, Kim TK, Kim EA, Joo SH, Pak C, Lee YH, Chang H (2008) Adv Mater 20:2341–2344
116. Hasani-Sadrabadi MM, Dorri NM, Ghaffarian SR, Dashtimoghadam E, Sarikhani K, Majedi FS (2010) J Appl Polym Sci 117:1227–1233
117. Doğan H, Inan TY, Koral M, Kaya M (2011) Appl Clay Sci 52:285–294
118. Duangkaew P, Wootthikanokkhan J (2008) J Appl Polym Sci 109:452–458
119. Deyrail Y, Mighri F, Bousmina M, Kaliaguine S (2007) Fuel Cells 07:447–452
120. Yang C-C, Lee Y-J (2009) Thin Solid Films 517:4735–4740